ELSEVIER

RESEARCH: Review

A molecular review on weakly solvating electrolytes for lithium batteries

Yao-Peng Chen [a], Xiang Chen [a,*], Nan Yao [a], Zhao Zheng [a], Legeng Yu [a], Yu-Chen Gao [a], Han-Bing Zhu [a], Chao-Long Wang [a], Jin-Hao Yao [a], Qiang Zhang [a,b,c,*]

[a] Tsinghua Center for Green Chemical Engineering Electrification (CCEE), Beijing Key Laboratory of Green Chemical Reaction Engineering and Technology, Department of Chemical Engineering, Tsinghua University, Beijing 100084, China
[b] Institute for Carbon Neutrality, Tsinghua University, Beijing 100084, China
[c] Shanxi Research Institute for Clean Energy, Tsinghua University, Taiyuan 030032, China

Carbonate-based electrolytes have significantly advanced the practical applications of lithium batteries (LBs) in various fields. However, commercial carbonate-based electrolytes exhibit sluggish desolvation behavior, resulting in poor performance of LBs under fast-charging and low-temperature conditions. In contrast, weakly solvating electrolytes (WSEs) have demonstrated rapid desolvation due to relatively weak Li^+–solvent interactions. This review summarizes the recent progress of molecular design strategies for WSEs. First, the origins and characteristics of WSEs are analyzed. The dielectric constant (ε) and donor number (DN) of solvents affect the interactions among Li^+, solvents, and anions, which are critical for the formation of WSEs. Both theoretical calculations and experimental characterizations are introduced to afford qualitative or quantitative WSE investigation. The solvent molecule design strategies for WSEs are summarized, including increasing steric hindrance, reducing the number of donor atoms, and reducing the negative charge on donor atoms. Finally, insightful perspectives are proposed to advance the development of WSEs in practical LBs.

Keywords: Lithium batteries; Weakly solvating electrolytes; Solvation structures; Molecular simulations; Solid electrolyte interphase

Introduction

Lithium (Li) ion batteries (LIBs) have been extensively applied in various practical applications, including electric vehicles, portable electronic devices, and large-scale smart grids [1–5]. Nevertheless, routine LIBs are falling short of meeting the increasing requirement for an energy density higher than 500 Wh kg^{-1}, primarily due to the limited specific capacity of graphite anodes (372 mAh g^{-1}) [6,7]. This limitation in energy density directly affects the range of electric vehicles. Consequently, there is an urgent need to explore emerging battery systems with ultrahigh energy density. Among available anode materials, Li metal stands out because of its very low electrode potential (−3.04 V *vs.* the standard hydrogen electrode) and ultrahigh theoretical specific capacity (3860 mAh g^{-1}) [8–14]. For cathodes, high-voltage materials such as Li-rich layered oxides and nickel-rich layered oxides are promising choices for increasing the battery energy density [15–22]. High-voltage Li metal batteries (LMBs) are anticipated to achieve ultrahigh energy density to address range anxiety. However, these systems encounter numerous challenges in advanced energy materials, emerging energy chemistry, and related device manufacture.

The reactions between organic electrolytes and Li metal anodes render the formation of solid electrolyte interphase (SEI) [23–27]. Chemically unstable and mechanically fragile SEIs can induce dendrite growth, further resulting in several issues:

* Corresponding authors at: Tsinghua Center for Green Chemical Engineering Electrification (CCEE), Beijing Key Laboratory of Green Chemical Reaction Engineering and Technology, Department of Chemical Engineering, Tsinghua University, Beijing 100084, China.
E-mail addresses: Chen, X. (xiangchen@mail.tsinghua.edu.cn), Zhang, Q. (zhang-qiang@mails.tsinghua.edu.cn).

https://doi.org/10.1016/j.mattod.2025.02.021

(1) cell short circuits, (2) aggravated adverse reactions, (3) evolution of dead Li from dendrites, and (4) large volume changes [28–30]. Similarly, a cathode electrolyte interphase (CEI) forms on a cathode surface. Loose CEIs can lead to cathode degradation, particularly under high-voltage conditions, further exacerbating the undesired reactions between the electrolyte and the cathode. Therefore, the formation of SEI and CEIs with excellent properties is important. The physicochemical properties of SEIs and CEIs, which are strongly determined by the electrolyte decomposition in a working battery, are crucial for the safe and efficient operation of high-voltage LMBs [31–35].

To address the aforementioned issues, many strategies have been proposed to design effective electrolytes, including designing novel electrolyte additives and organic solvents and optimizing the salt concentration [36–41]. In particular, high-concentration electrolytes (HCEs) (3–5 M) and localized high-concentration electrolytes (LHCEs) have been distinguished for their ability to form SEIs and CEIs that are rich in inorganic components (LiF, Li_2O, and Li_3N) by increasing the salt concentration to incorporate anions into Li^+ solvation shells [42–45]. Inorganic-rich SEIs have demonstrated high Li plating and stripping Coulombic efficiency (CE) [46]. Inorganic-rich CEIs render improved compatibility with high-voltage cathodes [46–48]. Despite significant progress, HCE still suffers from high viscosity and cost. LHCE addresses the challenges of high viscosity and cost, but current diluents primarily consist of low-boiling-point fluorinated ethers, which limits its high-temperature applications [39].

Recently, weakly solvating electrolytes (WSEs) have been proposed to produce a solvation structure similar to that of HCEs and LHCEs at low salt concentrations. These WSEs have shown excellent performance in high-voltage LMBs. For instance, Li et al. [49] demonstrated that selective methylation of 1,2-dimethoxyethane (DME) α-H atoms can simultaneously increase the Li plating and stripping CE to over 99.7% and improve the anodic stability of working electrolyte up to 5.0 V. Methylation enhances the steric hindrance of the solvent, resulting in increased contact ion pairs (CIPs) and aggregates (AGGs), which promotes the formation of LiF-rich SEIs and alleviates the electrolyte decomposition. Unlike HCEs and LHCEs, WSEs reduce the interactions between Li^+ and solvent molecules to allow anions to enter the Li^+ solvation shells. Meanwhile, this weakened interaction between Li^+ and solvent molecules can facilitate the desolvation process of Li^+ [50]. As a result, WSEs are also utilized in low-temperature and fast-charging batteries. For instance, Ma et al. [51] reported that using dimethoxymethane (DMM) as a solvent for low-temperature LMBs allows for uniform Li deposition morphology and high plating and stripping efficiency (97.87% at −40°C). In addition to the inorganic-rich SEIs formed by the anion-rich solvation structures, the rapid desolvation process also contributes to uniform and efficient Li deposition. Since Zhang and co-workers [52] firstly proposed the concept of WSEs in 2021, these electrolytes have exhibited excellent performance under high-voltage, fast-charging, and low-temperature conditions [53–57]. Recently, the design principles of WSEs have been reviewed, focusing on the selection of Li salts and solvents in the electrolytes [58–61]. However, the design mechanisms of solvent molecules for WSEs still require further discussion. While the number of Li salts is limited, there is a vast array of solvent molecules available.

This review aims to afford insights into the molecular design of WSEs. First, the characteristics of WSEs are analyzed, including the weak solvating power of solvents and anion-rich solvation structures. Next, characterization methods for WSEs are introduced, encompassing Fourier transform infrared spectroscopy (FTIR), Raman spectroscopy, nuclear magnetic resonance (NMR), density functional theory (DFT), and molecular dynamics (MD) simulations. Subsequently, solvent molecule design strategies for WSEs are summarized, focusing on ethers, epoxides, fluorinated ethers, fluorinated esters, and siloxanes. Finally, insightful perspectives on electrolyte design are presented to promote the practical applications of WSEs in rechargeable batteries.

Characteristics of WSEs

WSEs refer to a situation where Li^+–solvent and Li^+–anion interactions are regulated to induce anion-dominated Li^+ solvation shells [34,60]. This anion-rich solvation structure can be achieved by weakening the Li^+–solvent interactions or enhancing the Li^+–anion interactions [62]. These interactions can be regulated by selecting appropriate Li salts and solvents. Consequently, WSE design strategies can be categorized into solvent engineering and salt engineering, with a primary focus on the former due to the limited variety of Li salts and the broader design space of solvents (Section 4) [63]. In solvent engineering, WSE typically employ solvents with weak solvating power while still ensuring the dissolution of Li salts. The key parameters for evaluating the solvating power of solvents include dielectric constant, donor number (DN), and electrostatic potential (ESP). A brief introduction to each parameter is provided as follows.

(1) Dielectric constant: The dielectric constant of a solvent is defined as the ratio of the capacitance of a capacitor using the solvent as the dielectric to the capacitance of the same capacitor in a vacuum. This value reflects the ability of solvents to weaken the Coulombic interactions between Li^+ and anions in Li salts. Solvents with a high dielectric constant can largely weaken interactions between Li^+ and anions in the electrolyte, generally leading to a strong solvating power [64–67]. For instance, ethylene carbonate (EC), with a dielectric constant of 89.6, possesses strong solvating power, whereas benzene exhibits weak solvating power with a dielectric constant of 2.3 [68].
(2) DN: The donor number of a solvent is defined as the standard molar reaction enthalpy of the solvent with antimony pentachloride in the 1,2-dichloroethane solvent. This value reflects the strength of interactions between donor atoms on solvent molecules and acceptor atoms. Solvents with a higher donor number usually deliver a stronger interactions with Li^+ and therefore exhibit a stronger solvating power [69–73]. For instance, DME and benzene, with a donor number of 20 and 0.1 kcal mol^{-1}, have strong and weak solvating power, respectively [74].
(3) ESP: Benzene has a low dielectric constant and donor number, leading to weak solvating power. However, for solvents like EC and DME, the relative solvating power cannot be

accurately determined by the dielectric constant or donor number alone. To address this, new parameters such as ESP [68], β value [75], and relative solvating power [76] have been proposed to describe solvating power. For instance, He et al. [68] proposed using ESP as a solvating power descriptor and employed $ESP_{min} - ESP_{max}$ plots to identify strong solvating solvents, weak solvating solvents, and anti-solvents.

Descriptors such as dielectric constant, DN, ESP, β value, and relative binding energy play a significant role in the quantitative description of solvating power. To accurately describe solvating power, new descriptors, including the geometric properties of solvents and anions, as well as solvent–anion and solvent–solvent interactions, can be further considered. The consideration of geometric properties is important because the space around Li^+ is limited. Solvent–anion and solvent–solvent interactions offer a complete understanding of the fundamental interactions within electrolytes. Solvating power is a complex phenomenon influenced by multiple interactions, requiring assessment with various descriptors. Symbolic learning, a powerful machine learning approach, can analyze this multidimensional data and identify key feature combinations for predicting solvating power.

Solvents with weak solvating power are beneficial for constructing an anion-rich solvation structure and forming WSEs. The relationships between descriptors, interactions, solvating power, and solvation structures remain unclear, and even the definition of solvating power varies. It is essential to clarify these relationships in detail (Fig. 1). Solvents (or anions) with a higher donor number indicate stronger Li^+–solvent and Li^+–anion interactions [77]. In contrast, the dielectric constant reflects the extent to which solvents weaken Li^+–solvent and Li^+–anion interactions [78]. Additionally, steric hindrance greatly affects Li^+–solvent and Li^+–anion interactions, as large steric hindrance prevents solvents from effectively binding with Li^+ [79]. Therefore, donor number, dielectric constant, and steric hindrance collectively determine Li^+–solvent and Li^+–anion interactions. The definition of solvating power remains ambiguous. Currently, Chen et al. [80] suggest that solvating power depends solely on the strength of Li^+–solvent (ion–dipole) interactions. The solvation structure results from the competitive coordination between solvents and anions with Li^+. WSEs exhibit both anion-rich solvation structures and weak solvating power, making them widely applicable in fast-charging, low-temperature, and high-voltage LBs.

Theoretical and experimental characterization methods for WSEs

The electrolyte is a crucial component of a working battery, influencing its safety, lifespan, fast-charging, and low-temperature performances. The bulk properties (solvation structure, Li salt solubility, and ionic conductivity, *etc.*) and interfacial properties (Li^+ desolvation, electrochemical window, *etc.*) depend on the fundamental cation–solvent, cation–anion, and anion–solvent interactions in electrolytes [81,82]. Interactions between Li^+ and solvents or anions affect the redox stability of the solvents and anions, further regulating the reaction behaviors of these components [83,84]. For instance, the compatibility of WSEs with Li metal renders the anion-rich solvation structure, which promotes the formation of inorganic-rich SEIs. Therefore, understanding fundamental interactions and solvation structures is essential to rational selection and design of working electrolyte. Theoretical calculations, such as DFT and MD, along with experimental techniques like NMR, FTIR, and Raman spectroscopy, can reveal the microstructure of electrolytes (Fig. 2). This section introduces various characterization methods and discusses their roles in addressing key scientific issues in WSE investigation.

(1) DFT: DFT obtains the charge density distribution of a system by solving the Schrödinger equation, thereby determining the ground state properties of the system. DFT has extensive applications in studying the static chemical properties of electrolytes. The difference in binding energy between Li^+–solvent and Li^+–anion affects the solvation structures and the solubility of Li salts [85]. ESP can be employed to identify the binding sites of solvents toward a Li^+ and predict the reactive sites within solvation structures [86]. The lowest unoccupied molecular orbital (LUMO) and the highest occupied molecular orbital (HOMO) energy levels are related to the redox stability of electrolyte components [87]. For instance, Chen et al. [78] elucidated the role of solvation effects in regulating Li salt solubility at an atomic level through DFT calculations. The solvation effects can weaken Li^+–solvent and Li^+–anion interactions, with the dielectric constant playing a crucial role. A larger binding energy between Li^+ and

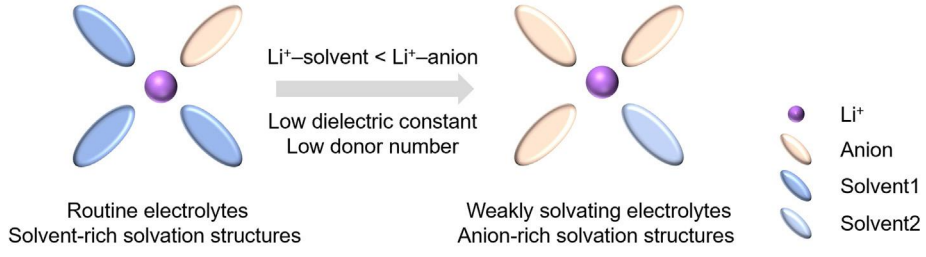

FIG. 1

The characteristics and key factors of WSEs. The donor number and dielectric constant are present as an example. Solvent1 and solvent2 represent strong solvating solvent and weak solvating solvent, respectively.

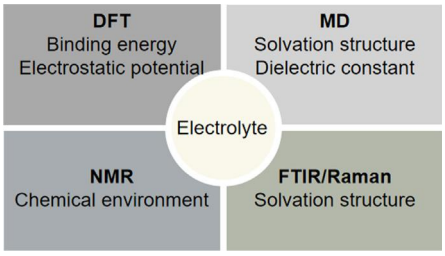

FIG. 2

Combining theoretical calculations and experimental techniques in WSE development.

anion can make Li salts more difficult to dissolve to some extent. Specifically, the dissolution behavior of lithium nitrate ($LiNO_3$) was predicted and further verified by experimental characterizations.

(2) MD: MD simulations obtain atomic trajectories by numerically solving motion equations for molecular systems based on classical mechanics. Statistical analysis of these trajectories affords insights into the dynamic properties of electrolytes [88–90]. Various physicochemical properties, such as dielectric constant, ionic conductivity, and diffusion coefficient, are typically determined experimentally, which is expensive and unfavorable for high-throughput screening of electrolytes. Yao et al. [91] calculated the dielectric constant of electrolytes via MD simulations and constructed a corresponding database to facilitate efficient electrolyte screening. Visualization of atomic trajectories offers fresh insights into the solvation structures [92–94]. While techniques such as NMR, FTIR, and Raman spectroscopy afford related information, they often lack comprehensive atomic-level understanding. Ravikumar et al. [95] employed MD simulations to investigate the impact of different concentrations (0.06–4.0 M) of EC–lithium hexafluorophosphate ($LiPF_6$) electrolytes on their transport and structural properties. Their findings indicate that increasing concentration shifts the predominant solvation structure from solvent separated ion pairs (SSIPs, Li^+ is surrounded by solvents) in dilute states to AGGs, significantly affecting the transport properties of the electrolytes.

(3) NMR: NMR uses the resonance of atomic nuclei with radio frequency electromagnetic waves in a strong electrostatic magnetic field to produce radio frequency electromagnetic spectra that reflect the internal structure of the sample. NMR can detect changes in the microstructure of electrolytes at an atomic scale and is widely employed in electrolyte studies [96,97]. For instance, Bogle et al. [98] used ^{17}O NMR to analyze Li^+–EC and Li^+–dimethyl carbonate (DMC) interactions in a series of 1.0 M $LiPF_6$ binary solvent mixtures of EC and DMC. It was observed that the most obvious changes in ^{17}O chemical shift occurred at the carbonyl oxygen of EC, indicating that Li^+ strongly prefers EC over DMC, primarily coordinating with carbonyl rather than ethereal oxygens. Unlike one-dimensional NMR, two-dimensional NMR can detect weak long-range interactions, such as anion–solvent and solvent–solvent interactions. Wahyudi et al. [99] have made a detailed review of the applications of two-dimensional NMR in electrolytes.

(4) FTIR and Raman spectroscopy: Both FTIR and Raman spectroscopy are categorized under molecular vibration spectroscopy. FTIR corresponds to the asymmetric vibration of polar groups, while Raman spectroscopy reflects the symmetric vibration of nonpolar groups. The two methods are effective in analyzing electrolyte microstructures, such as the changes in Li^+ solvation shells and anion coordination structures [100–102]. For instance, Efaw et al. [103] employed Raman spectroscopy to reveal unique micellar structures presented in LHCEs, where solvents function as surfactants between insoluble salts in the diluent. When LiFSI is dissolved in DME, the C–O stretching vibration (820–850 cm^{-1}) of pure DME reduces, and blue shifts to 873–877 cm^{-1}, corresponding to the interactions between Li^+ and ether oxygen atoms. DME and tris(2,2,2-trifluoroethyl)orthoformate (TEFO) are miscible, while LiFSI exhibits minimal solubility in TEFO. Raman spectroscopy confirms the observation by demonstrating that peaks in the 820–870 cm^{-1} range are retained in both TFEO and LHCE.

Although DFT, MD simulations, NMR, FTIR, and Raman spectroscopy all have unique advantages in probing the solvation structures of WSEs, each method has its own limitations. In order to have a comprehensive understanding of the solvation structures and the interactions, it is important to combine the aforementioned methods. The following section focuses on the design strategies of solvent molecules for WSEs, offering a detailed analysis of how these technologies work together to enhance our understanding of the solvation structures of WSEs.

Design strategies of solvent molecules for WSEs

Solvent molecule design for WSEs requires a comprehensive understanding of both molecular characteristics and solvent properties. From a mechanistic perspective, the key to designing solvent molecules for WSEs lies in weakening the Li^+–solvent interactions. At the molecular level, factors including steric hindrance of solvent molecules and the type, number, and negative charge of the coordinating atoms can be considered. Molecules with large steric hindrance hinder the coordination of Li^+ with solvent molecules. The coordination ability of different atoms varies, with O atoms generally having stronger coordination abilities with Li^+ compared to F atoms. Furthermore, molecules with more than two coordinating atoms can form chelation interactions between Li^+ and solvent molecules. The interactions between Li^+ and solvent molecules are primarily electrostatic, and the charge of the coordinating atoms plays a crucial role in determining the coordination strength. At the solvent level, important parameters such as DN and dielectric constant can be considered. DN is a thermodynamic parameter that reflects the steric hindrance of the solvent molecules as well as the type, number, and negative charge of the coordinating atoms. The dielectric constant indicates the extent to which the Li^+–solvent and Li^+–anion interactions are weakened. In the following section, we summarize five design strategies for specific solvent

molecules in WSEs, taking into account these molecular and solvent-level factors.

Linear ether solvent molecules

Regulating the chelation of solvent molecules and increasing the steric hindrance of solvent molecules are two key strategies for designing ether-based WSEs. Chelation refers to the process where two or more coordinating atoms (such as O) within the same ligand coordinate with a single metal ion (such as Li^+), forming a cyclic complex known as a chelate. Chelation can enhance the interactions between Li^+ and solvents. Therefore, weakening or eliminating the chelation effect is a crucial approach in the rational design of solvent molecules for ether-based WSEs. Ether solvent molecules with only one O atom do not form chelates when interacting with Li^+, generally resulting in weak solvating power [104–108]. For instance, Ma et al. [109] reported a WSE based on the butyl methyl ether (BME) solvent, which demonstrated compatibility with both sulfurized polyacrylonitrile (SPAN) cathode and Li metal anode. Compared to DME, the interactions between BME and Li^+ are weaker, due to its characteristic of possessing only one O atom. Specifically, the binding energy of Li^+–DME (−2.84 eV) is much larger than that of Li^+–BME (−1.74 eV) according to DFT calculations (Fig. 3a). Additionally, NMR fitting indicates that the DN of BME (16.6 kcal mol^{-1}) is lower than that of DME (20.0 kcal mol^{-1}). The DFT and NMR results collectively suggest that the interactions between Li^+ and BME is weaker than that between Li^+ and DME. Raman spectroscopy was further employed to investigate the differences in the solvation structures of the two electrolytes. Specifically, the spectral region between 700 and 780 cm^{-1}, corresponding to the S–N–S stretching vibration, was analyzed. Compared to the 1.0 M LiFSI BME electrolyte, the 1.0 M LiFSI DME exhibited a red shift of the S–N–S stretching vibration peak, which can be attributed to the presence of more free FSI^-. MD simulations further explored the solvation structure of the electrolytes, revealing that the FSI^- coordination number in 1.0 M LiFSI DME and 1.0 M LiFSI BME electrolytes is 0.2 and 1.8, respectively. Ethers containing a single O atom are typical weakly solvating solvents widely used in low-temperature and fast-charging applications [105,107,108].

In addition to preventing the formation of chelates, weakening the chelation effect can also aid in designing solvents with weak solvating power. The strength of the interactions between Li^+ and solvents is related to the size of the chelate ring. It is generally agreed that five-membered and six-membered rings are relatively stable. Therefore, for ethers containing two O atoms, the solvating power can be adjusted by changing the number of C atoms between the two O atoms for ethers containing two O atoms [111–113]. Ma et al. [111] reported a DMM-based electrolyte with a weak solvating power, which exhibits a low desolvation energy. DMM has a low dielectric constant of 2.7, making it a potential weakly solvating solvent. The binding energy of Li^+–DMM (−2.57 eV) is lower than that of Li^+–DME (−2.84 eV), which can be explained by the stability of the complex formed by solvent and Li^+ (Fig. 3c). Specifically, Li^+–DMM forms a four-membered ring structure, which is less stable compared to the five-membered ring structure formed by Li^+–DME. Subsequently, LiFSI was dissolved in both solvents to form 1.0 M electrolytes. The ^{17}O peak of 1.0 M LiFSI DMM shifts upfield compared to that of 1.0 M LiFSI DME, indicating stronger Li^+–anion interactions in the DMM electrolyte (Fig. 3d). According to MD simulations, the solvation structures of DMM and DME are $Li^+(DMM)_{1.2}(FSI^-)_{1.7}$ and $Li^+(DME)_{1.5}(FSI^-)_{1.4}$, respectively. Compared to the DME electrolyte, the DMM electrolyte with solvation shells containing fewer and weaker coordinating solvents renders faster desolvation kinetics. Electrochemical impedance spectroscopy (EIS) was employed to determine the activation energy of the desolvation process for the DMM and DME systems, which were 54.37 and 53.18 kJ mol^{-1}, respectively (Fig. 3e). Due to the anion-rich solvation structure and rapid desolvation process, Li||LTO full cells using 1.0 M LiFSI DMM exhibit excellent low-temperature performance. The capacity retention of the full cell with DMM electrolyte is 75.9% after 100 cycles at −20°C. In contrast, DMM is only 26.1% after 60 cycles (Fig. 3f). Furthermore, increasing the number of C atoms between the two O atoms of DME can also adjust the solvating power. For instance, Li^+–1,3-dimethoxypropane (DMP) forms a six-membered ring structure, which has a solvating power similar to that of DME [111,112]. However, if the number of C atoms is further increased to four (1,3-dimethoxybutane (DMB)), a seven-membered ring structure with Li^+ is produced, resulting in relatively weak solvating power [112].

Ethers containing a single O atom do not form chelates with Li^+, resulting in weak solvating power. Ethers with two O atoms can form five-membered rings or six-membered rings with Li^+, which are relatively stable. By increasing or decreasing the number of C atoms between the two O atoms in ethers, solvents with weak solvating power can be modulated. When considering ethers with more than two O atoms, the solvating power of diethylene glycol dimethyl ether (G2) and triethylene glycol dimethyl ether (G3) increases, which is caused by the formation of multiple rings by Li^+–G2 and Li^+–G3 [114–118]. However, tetraethylene glycol dimethyl ether (G4) exhibits weak solvating power, which is attributed to the steric effects [119].

In a coordination compound, the introduction of a large functional group into a ligand (such as a solvent) generates steric hindrance, which affects the formation of a coordination compound with the central atom (such as Li^+). Methylation, ethylation, or propylation of ether solvent molecules can reduce their solvating power [110,120–127]. On one hand, methyl, ethyl, and propyl are weakly electron-donating groups and have little impact on the O atomic charge in the solvent molecules. On the other hand, these groups exhibit a large steric hindrance, which weakens the Li^+–solvent interactions. Eunseok et al. [110] reported the design of a large-steric and low-dielectric constant (5.5) ether solvent, 1,2-dimethoxypropane (DMP1), which is capable of reliably operating LMBs with high-voltage (4.3 V) cathode. Compared to DME, DMP1 renders a smaller dipole moment (1.22 < 1.49) and dielectric constant (5.5 < 6.9), indicating that DMP1 has a weaker solvating power. Although the additional weakly electron-donating methyl group increases the overall electron density of the system, its steric effect limits the interactions between DMP1 and Li^+ (Fig. 3b). To verify whether the electrostatic interactions between DMP1 and Li^+ were indeed weakened compared to that of DME, DFT calculations were performed. ESP_{min} of DMP1 was calculated to be −166 kJ mol^{-1},

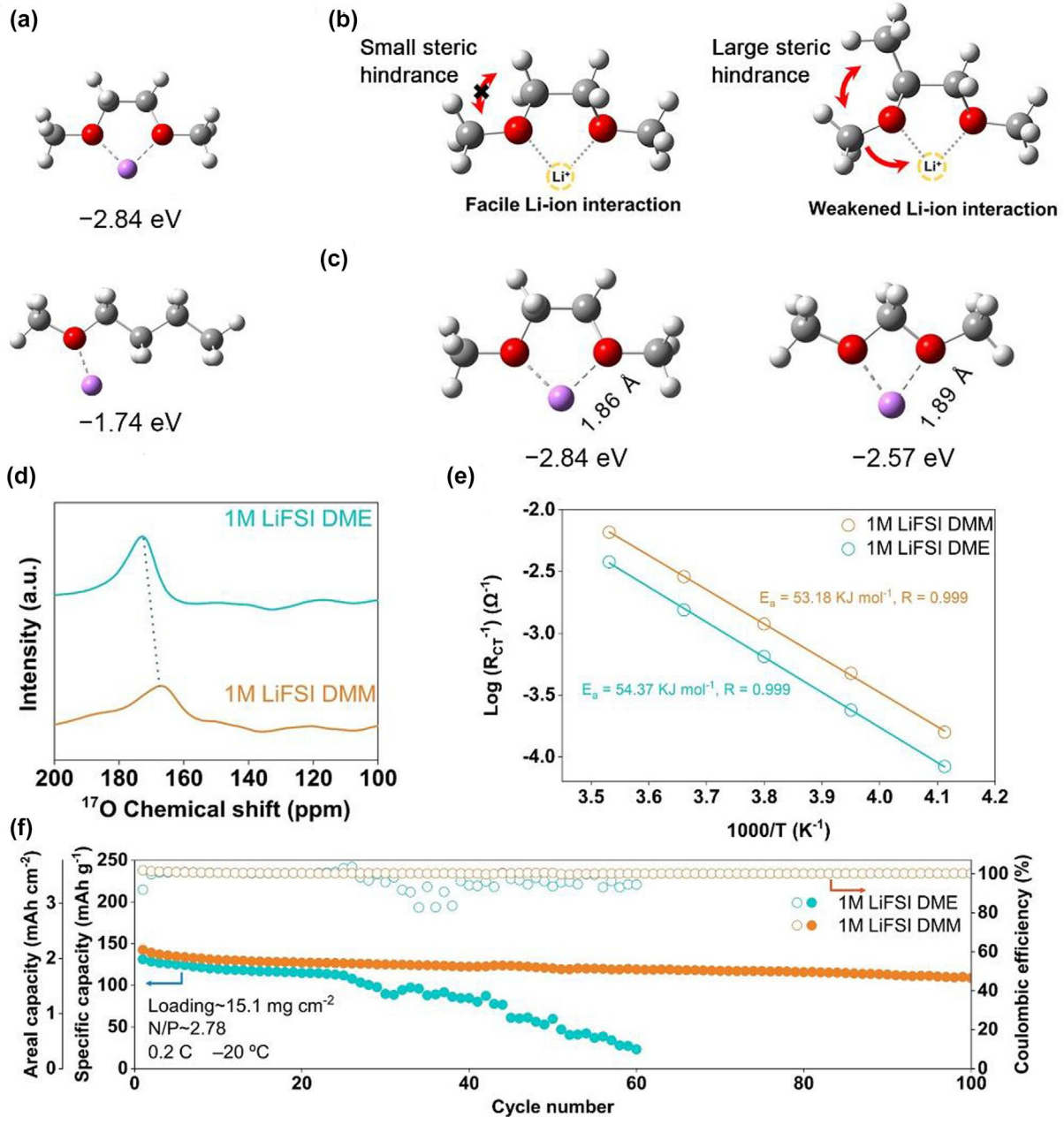

FIG. 3

The design principles, properties, and performances of linear ether electrolytes. (a) Chelation effect (Reprinted with permission from Ref. [109]. Copyright 2023, Wiley-VCH GmbH.). (b) Steric hindrance (Reprinted with permission from Ref. [110]. Copyright 2022, American Chemical Society.). (c) Chelation ring (Reprinted with permission from Ref. [111]. Copyright 2022, Wiley-VCH GmbH.). (d) ^{17}O NMR spectra of different electrolytes (Reprinted with permission from Ref. [111]. Copyright 2022, Wiley-VCH GmbH.). (e) Li^+ desolvation energy (Reprinted with permission from Ref. [111]. Copyright 2022, Wiley-VCH GmbH.). (f) Cycle performance of Li||lithium titanate (LTO) full cells (Reprinted with permission from Ref. [111]. Copyright 2022, Wiley-VCH GmbH.).

which is smaller than that of DME (−176 kJ mol^{-1}), indicating a weakened solvating power compared to DME. Subsequently, the solvation structure properties of 2.0 M LiFSI DME and 2.0 M LiFSI DMP1 electrolytes were investigated. The ^7Li peak of 2.0 M LiFSI DMP1 was shifted upfield compared to that of 2.0 M LiFSI DME. The upfield ^7Li chemical shift indicates a larger number of anions surround the Li^+ in DMP1-based electrolytes than in their DME analogs, owing to the increased electron density surrounding the ^7Li nuclei.

Epoxide solvent molecules

Compared to linear ethers, cyclic ether solvent molecules exhibit different characteristics. Cyclic ether solvent molecules containing two O atoms within the ring structure do not produce chelates with Li^+, a consequence of the inherent rigidity of the ring structure. Therefore, the intrinsic characteristics of cyclic ether solvent molecules result in weak solvating power [128–133]. Yao et al. [129] reported a WSE composed of a purely non-polar solvent, 1,4-dioxane (1,4-DX), which leads to a unique

solvation structure where ion pairs and aggregates predominate, even at a low salt concentration of 1.0 M. Despite moderate ε, DME exhibits the largest solvating power among the three solvents, due to its large DN (20 kcal mol^{-1}) and chelating effect. In contrast, 1,3-DX displays low solvating power due to the steric hindrance imposed by its cyclic structure. 1,4-DX exhibits extremely weak solvating power, which is attributed to its ultra-low ε of 2.2 (Fig. 4a). To further explore the solvation structure, Raman spectra were obtained for three ether electrolytes. The S–N–S binding signal in FSI^- anion can be classified into the free anion (FA, 719 cm^{-1}), CIP (731 cm^{-1}), and AGG (742 cm^{-1}) (Fig. 4b). Among the three electrolytes, 1,4-DX has the highest proportion of the sum of CIP (35.4 %) and AGG (49.0 %), which aligns with the observed in relative binding energy ($E_S - E_A$, E_S: the binding energy of Li^+–anion, and E_A: the binding energy of Li^+–solvent). The descriptor of $E_S - E_A$ is proposed as a predictive tool for determining the actual solvation structure in different electrolytes. A larger $E_S - E_A$ value indicates that the CIP and AGG are preferentially formed over Li^+–solvent complexes, meaning that anions dominate the coordination competition over solvents. As a result, WSE + 2% EC enables ultra-stable cycling of the graphite electrode, with a 92% capacity retention after 500 cycles (Fig. 4c).

Fluorinated ether solvent molecules

Fluorination refers to the replacement of H atoms in solvent molecules with F atoms. The properties of F and H atoms are different [134,135]. Firstly, the electronegativity of a F atom (3.98) is much larger than that of a H atom (2.18), leading to a change in the surface charge distribution of solvent molecules after fluorination. Secondly, the radius of a F atom (64 pm) is larger than that of a H atom (37 pm), resulting in a change in the geometric shape of the solvent molecules. Consequently, fluorinated solvent molecules exhibit different physicochemical properties, such as solvating power and redox stability [136–140]. Li^+ typically interacts with O atoms (–O– in ethers and =O in esters) in solvent molecules. For fluorinated solvent molecules, the high electronegativity of F reduces the charge on the O atoms and thus weakens the Li^+–O interactions. Additionally, interactions between Li^+ and F atoms can occur, depending on the degree of fluorination (*e.g.*, $–CH_3$, $–CH_2F$, $–CHF_2$, and $–CF_3$) [141,142]. The strength of the interactions between Li^+ and fluorinated solvent molecules is significantly affected by the number and position of F atoms, which, in turn, influences the solvating power of the solvent.

There is no doubt that the Li^+–O interactions are weakened after fluorination. However, the existence of interactions between Li^+ and F atoms remains uncertain. Currently, it is generally believed that Li^+ interacts with the F atoms on $–CH_2F$ and $–CHF_2$, but not with the F atoms on $–CF_3$ [143] (Fig. 5a). Yu et al. [144] synthesized fluorinated 1,4-dimethoxylbutane (FDMB), which demonstrated a unique Li^+–F interactions and led to high anion content in the Li^+ solvation sheath. When LiFSI is dissolved in DME (or DMB), only a colorless solution is obtained. However, the solution with FDMB showed a brown color, suggesting the presence of unique Li^+–solvent interactions in FDMB electrolytes. To verify this coordination, a signal crystal of lithium triflate (LiTf) co-crystallized with FDMB was obtained. The crystal structure demonstrates that the $Li–F_{FDMB}$ (2.94 Å) dis-

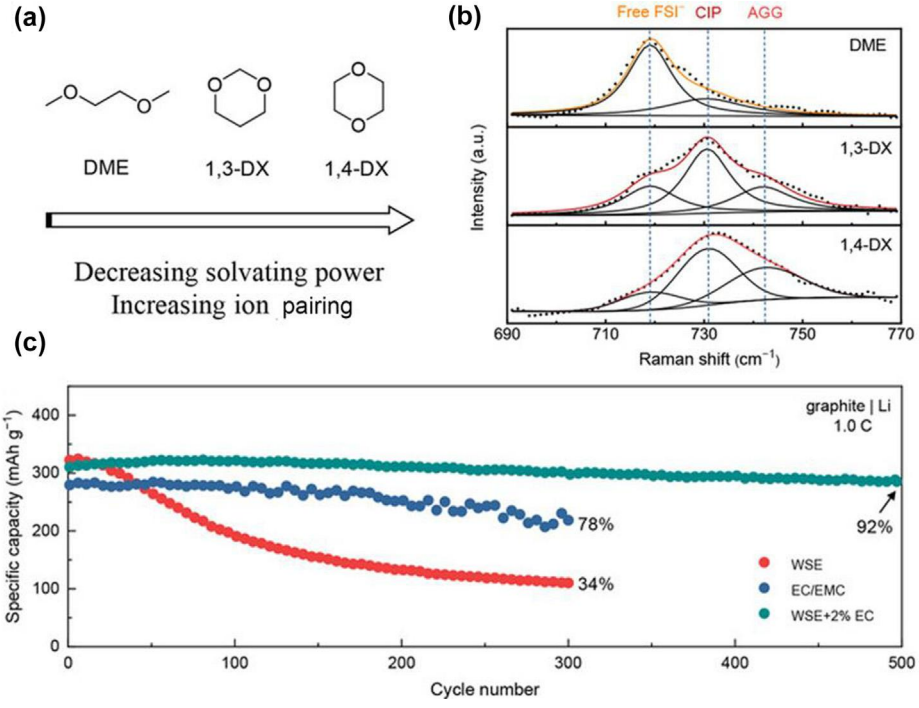

FIG. 4

The design principles, properties, and performances of epoxide electrolytes. (a) The ranking of the solvating power of solvents from high to low (Reprinted with permission from Ref. [129]. Copyright 2020, Wiley-VCH GmbH.). (b) Raman spectra of 1.0 M LiFSI dissolved in various solvents (Reprinted with permission from Ref. [129]. Copyright 2020, Wiley-VCH GmbH.). (c) Long-term cycling performance (Reprinted with permission from Ref. [129]. Copyright 2020, Wiley-VCH GmbH.).

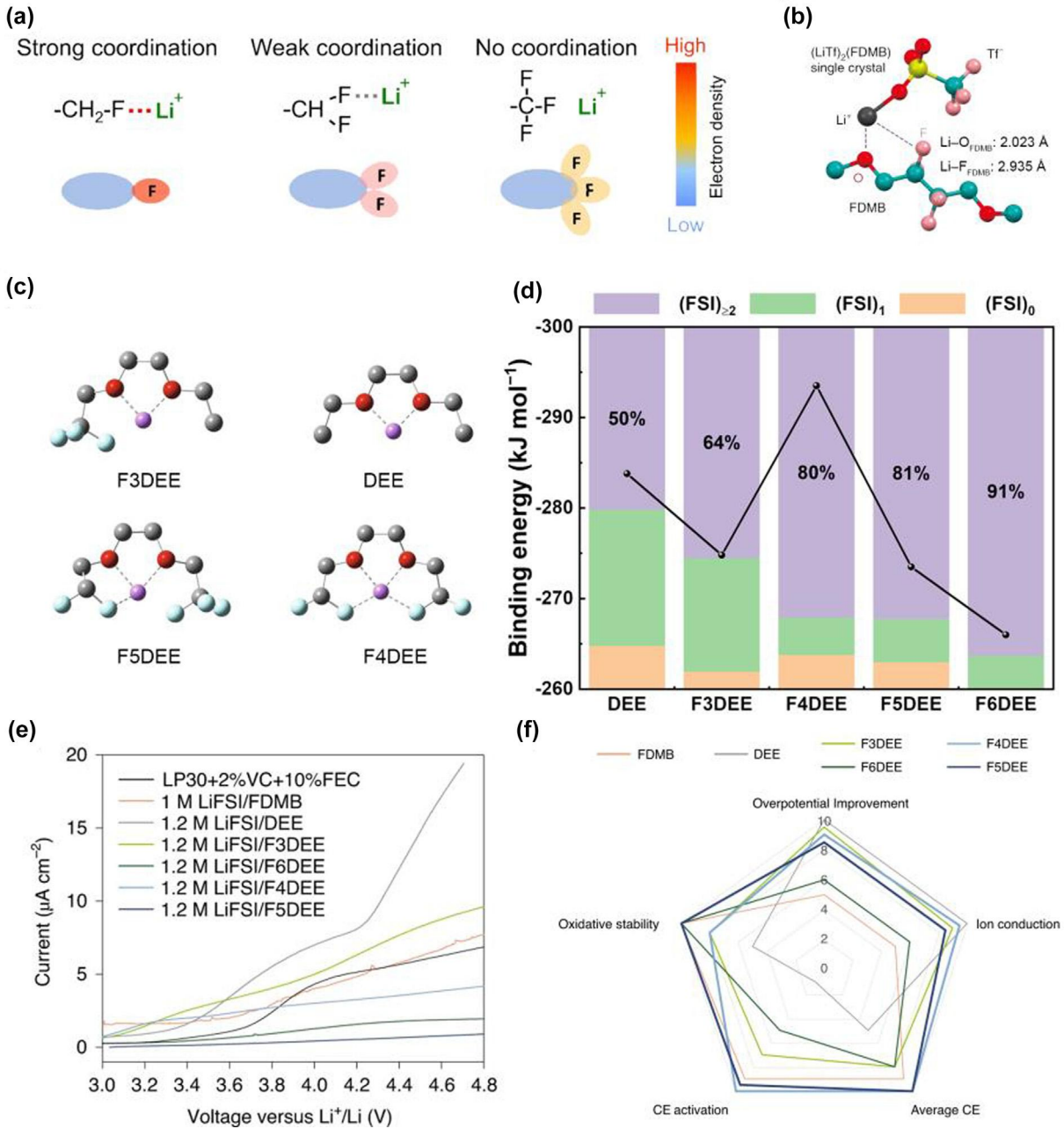

FIG. 5

The design principles, properties, and performances of fluorinated ether electrolytes. (a) Coordination chemistry of monofluoride, difluoro-, and trifluoro-groups (Reprinted with permission from Ref. [143]. Copyright 2023, Springer Nature.). (b) Single crystal of LiTf/FDMB showing Li–F interactions. For clarity, only one LiTf and one FDMB are shown (Reprinted with permission from Ref. [144]. Copyright 2020, Springer Nature.). (c) Coordination structures of Li^+–solvent complexes. Color scheme of atoms: Li–purple, C–gray, H–white, O–red, F–light blue (Reprinted with permission from Ref. [145]. Copyright 2022, Springer Nature.). (d) Binding energy of Li^+–solvent complexes and the proportion of solvation configurations with different amounts of FSI^- anions in Li^+-centric structures (Reprinted with permission from Ref. [145]. Copyright 2022, Springer Nature.). (e) Linear sweep voltammetry of Li||Al half cells to show anodic stability and tolerance to Al corrosion (Reprinted with permission from Ref. [145]. Copyright 2022, Springer Nature.). (f) Radar plot evaluating the developed electrolytes (Reprinted with permission from Ref. [145]. Copyright 2022, Springer Nature.).

tance in FDMB is similar to the $Li–O_{FDMB}$ (2.02 Å) distance in FDMB, indicating a weak yet existing interaction between Li^+ and F atoms on FDMB (Fig. 5b). ESP calculations further reveal that the negative charge distribution is solely concentrated on O atoms in DME and DMB. However, the negative charge is distributed on both O and F atoms of FDMB, facilitating coordination with Li^+. MD simulations were employed to explore the solvation structure. Unlike in DME and DMB, a five-membered ring was observed in the LiFSI/FDMB system, where Li^+ is simultaneously coordinated with both O_{FDMB} and F_{FDMB} atoms. Additionally, the FSI^-/solvent ratio in the Li^+ solvation shells is the highest in 1.0 M LiFSI FDMB at 3.29:1 (compared to 2.31:1 in 1.0 M LiFSI DME and 2.29:1 in 1.0 M LiFSI DMB), indicating that FDMB has weak solvating power. The weak solvating power of

FDMB was also verified by the dominance of the uncoordinated ether band (free solvent) in the FTIR of 1.0 M LiFSI FDMB electrolytes.

A comprehensive understanding of the Li^+–F interactions affords a microscopic insight into the design of solvents for WSEs through fluorination strategy. To design fluorinated ether-based WSEs rationally, the position and degree of fluorination are further considered, as these factors are closely related to the solvent's solvating power and the electrolyte's solvation structure. Fluorination can be categorized according to the position of the F atoms, such as α-fluorination, β-fluorination, and γ-fluorination. For ethers, α-fluorination dramatically reduces molecular polarity and solvating power, resulting in almost no solubility for Li salts [47,146–148]. Consequently, such fluorinated ethers are typically used as diluents and are unsuitable as solvents for WSEs. In contrast, γ-fluorination has a smaller effect due to its relatively long distance from the –O– group. Therefore, only β-fluorination can maintain the balance of the solvating power in fluorinated ether solvents, making it a more viable option for WSE applications.

In addition to the fluorinated position, the degree of fluorination also determines the solvating power of fluorinated ether solvents. Highly fluorinated ethers exhibit poor solubility with Li salts and are generally used as diluents in HCE and LHCE systems [149]. Therefore, achieving an optimal degree of fluorination is crucial for designing effective fluorinated ether. Yu et al. [145] reported a series of WSEs with different fluorination degrees based on fluorinated 1,2-diethoxyethane (DEE), specifically 2-(2-ethoxyethoxy)-1,1,1-trifluoroethane (F3DEE), 2-[2-(2,2-difluoroethoxy)ethoxy]-1,1-difluoroethane (F4DEE), 2-[2-(2,2-difluoroethoxy)ethoxy]-1,1,1-trifluoroethane (F5DEE), and 1,1,1-trifluoro-2-[2-(2,2,2-trifluoroethoxy)ethoxy]ethane (F6DEE). The fluorination positions were all at the β-position, consistent with the previous analysis. DFT calculations were performed to determine optimized binding configurations between Li^+ and each type of solvent molecule. The Li^+ showed a stronger interaction (i.e. shorter Li–F distance) with $–CHF_2$ than with $–CF_3$ (Fig. 5c). As the number of F atoms increases, the binding energy of the Li^+–solvent complex initially increases and then reduces (Fig. 5d). The volcano trend ascribed to that F4DEE has two $–CHF_2$ groups, which result in strong Li–F interactions. MD simulations were further conducted to investigate the Li^+ solvation structure. The distribution of Li^+ solvates, including the percentages of solvent surrounded Li^+ (SSL), Li^+–anion single pair (LASP), and Li^+–anion cluster (LAC), was analyzed. Each of these solvates features a distinct number of Li^+-coordinating anions of 0, 1, and ≥2 in the primary solvation sheath, respectively. As the number of F atoms increases, the proportion of LAC gradually increases, indicating a reduction in the degree of ion dissociation (Fig. 5d). Furthermore, all fluorinated DEE electrolytes demonstrated greater stability against oxidation compared with DEE electrolytes, a property related to anion-rich solvation structures (Fig. 5e). It is worth noting that all the fluorinated DEE should be classified as weakly solvating solvents. However, the fine-tuning of fluorination allows for a balance among various properties (Fig. 5f).

Fluorinated ester solvent molecules

Similar to fluorinated ethers, the fluorination of esters reduces the polarity of ester solvents, resulting in a reduction in the solvating power [151–162]. The strength of the Li^+–fluorinated ester interactions is determined by both Li^+–O and Li^+–F interactions in fluorinated esters. A higher degree of fluorination, along with the proximity of the F atom to the –C═O group induces a less negative charge on the O atom (–C═O) and weakens the Li^+–O interactions. Yoo et al. [163] reported a series of fluorinated ethyl acetates (EAs), including trifluoroethyl acetate (EA-f), ethyl trifluoroacetate (f-EA), and trifluoroethyl trifluoroacetate (f-EA-f). From EA, EA-f (α-fluorinated), and f-EA (γ-fluorinated) to f-EA-f, the negative charge on the O atoms were −0.600, −0.583, −0.547, and −0.530, respectively, indicating gradual weakening of the Li^+–solvent interactions. The fully fluorinated $–CF_3$ group is symmetric and lacks a local dipole, whereas $–CH_2F$ and $–CHF_2$ groups are locally polar, which is beneficial for the dissolution of Li salts and the transport of Li^+ in the electrolytes [164]. Mo et al. [150] reported a family of EAs, including ethyl fluoroacetate (EFA), ethyl difluoroacetate (EDFA), and ethyl difluoroacetate (ETFA), where the moderately fluorinated EDFA enables fast-charging and low-temperature LIBs. ^{19}F NMR was conducted to investigate whether Li^+ interacts with F atoms in fluorinated-EAs. The ^{19}F peak shows an upfield shift when LiFSI is introduced into EFA (or EDFA), but almost no shift when LiFSI is introduced into ETFA, indicating that there is no Li^+–F interaction in ETFA electrolytes (Fig. 6c). As demonstrated in Fig. 6a, the Li–F bond length increases with the degree of fluorination. The Li^+–F and Li^+–O interactions together determine the binding energy of Li^+–solvent, which firstly increases and then reduces from EA, EFA, and EDFA to ETFA (Fig. 6b). The solvation structure was studied using Raman spectroscopy, analyzing the different forms of anions based on their Raman peaks. In the four different electrolytes, both CIPs and AGGs gradually appeared as the number of F atoms increased (Fig. 6d). MD simulations were also conducted to quantitatively analyze Li^+-centric cluster structures, and the results were consistent with the Raman spectroscopy findings (Fig. 6b). These results indicate that the solvating power and solvation structure can be modulated by adjusting the number of F atoms, which further affects the electrolyte properties and battery performances. The 1.2 Ah NCM811||Gr pouch cells with EDFA–fluoroethylene carbonate (FEC) electrolytes exhibit excellent rate capability, maintaining 83% capacity at 0.2 C. Besides, 75 and 60% capacity at −30°C and −40°C, respectively. The excellent performances at both room and low temperatures are attributed to the weak solvating power and anion-rich solvation structure (Fig. 6e, f).

Siloxane solvent molecules

Siloxane is an emerging WSE, of which the weak solvating power characteristic is attributed to the silicon (Si) atoms. Unlike a C atom, a Si atom is typically bonded to $–C_nH_{2n+1}$ and $–OC_nH_{2n+1}$ instead of H atoms. This configuration results in solvent molecules with large steric hindrance and small dielectric constant such as tetraethyl orthosilicate (TEOS), methyltriethoxysilane (MTES), dimethyldiethoxysilane (DMES), and dimethyldimethoxysilane (DMMS) [165–176]. Huang et al. [167] designed a DMMS electrolyte *via* a robust bond strategy for high-voltage LMB. The Si–O bond in DMMS contributes to a broader electrochemical window and enhanced chemical stability compared with routine solvents like DME and EC

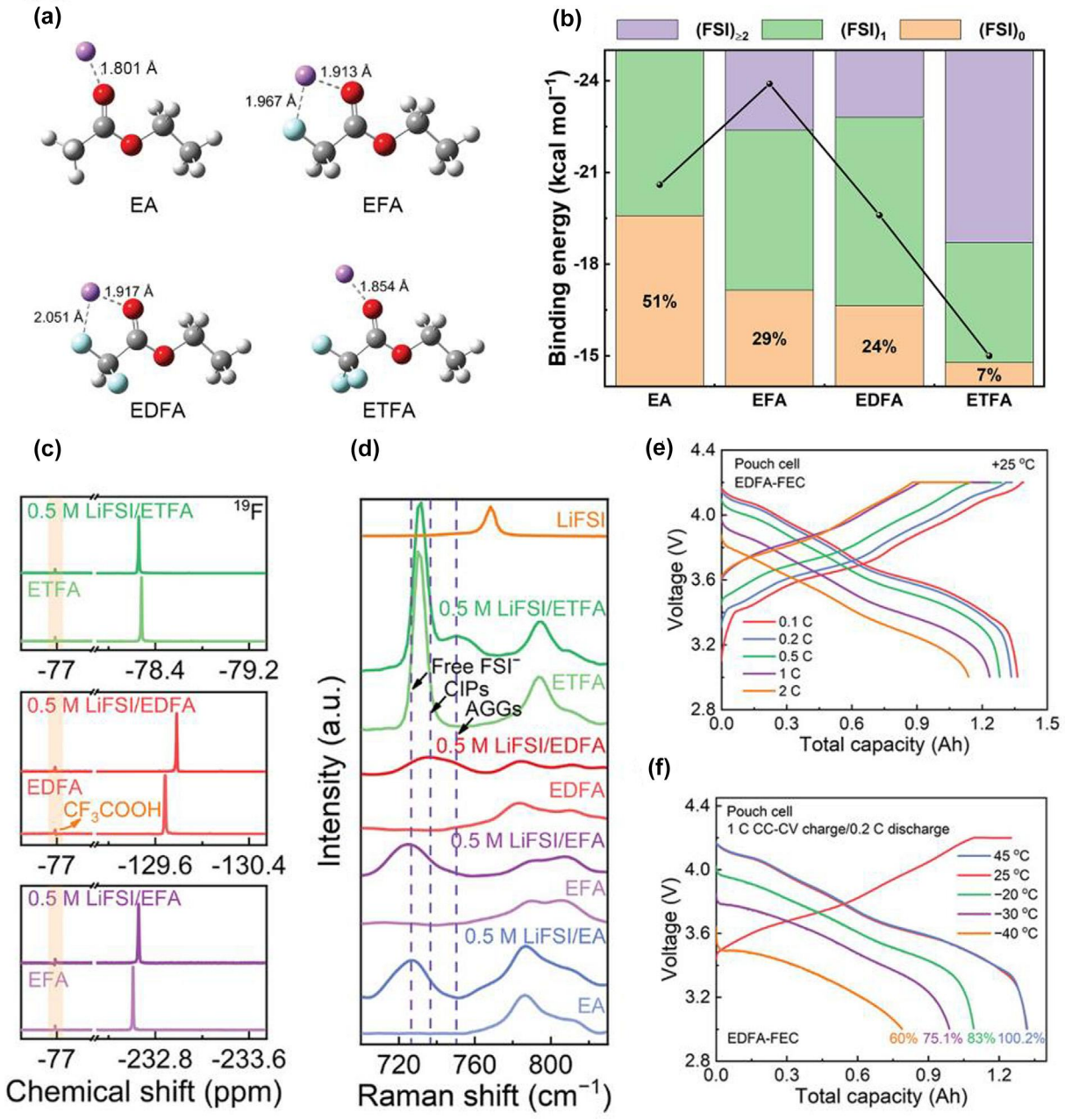

FIG. 6

The design principles, properties, and performances of fluorinated ester electrolytes. (a) Coordination structures of Li^+–solvent complexes. Color scheme of atoms: Li–purple, C–gray, H–white, O–red, F–light blue (Reprinted with permission from Ref. [150]. Copyright 2023, Wiley-VCH GmbH.). (b) Binding energy of Li^+–solvent complexes and the proportion of solvation configurations with different amounts of FSI^- anions in the Li^+-centric structures (Reprinted with permission from Ref. [150]. Copyright 2023, Wiley-VCH GmbH.). (c) ^{19}F NMR with CF_3COOH/D_2O as internal standard (Reprinted with permission from Ref. [150]. Copyright Wiley-VCH GmbH.). (d) Raman spectra of EA-based solvents and 0.5 M LiFSI in EA solvents (Reprinted with permission from Ref. [150]. Copyright Wiley-VCH GmbH.). (e) Rate performance (Reprinted with permission from Ref. [150]. Copyright Wiley-VCH GmbH.). (f) Wide-temperature performance (Reprinted with permission from Ref. [150]. Copyright Wiley-VCH GmbH.).

(Fig. 7a). In practical electrolytes, the redox behavior of solvent is regulated by interactions with both Li^+ and anions [177–181]. To evaluate the redox behavior of various electrolytes, it is essential to analyze Li^+-centric and solvent-centric cluster structures. In the Li^+-centric cluster structures of different electrolytes, 1.5 M LiFSI DMMS exhibits the highest average anion coordination number of 2.81 (Fig. 7b). This anion-rich solvation structure is conducive to the formation of F- and O-rich SEI, effectively preventing solvent decomposition. As demonstrated in Fig. 7b, the CE of Li anodes increases with the rise of the average anion coordination number. Within the solvent-centric cluster structures of various electrolytes, DMMS demonstrates a higher oxidation potential, strategically eliminating the most vulnerable Sol-A cluster against oxidation (Fig. 7c–e). Due to the unique solvation structures, the 1.5 M LiFSI DMMS electrolyte, without any additive, enabled Li||NCM811 coin cells to retain 80% initial dis-

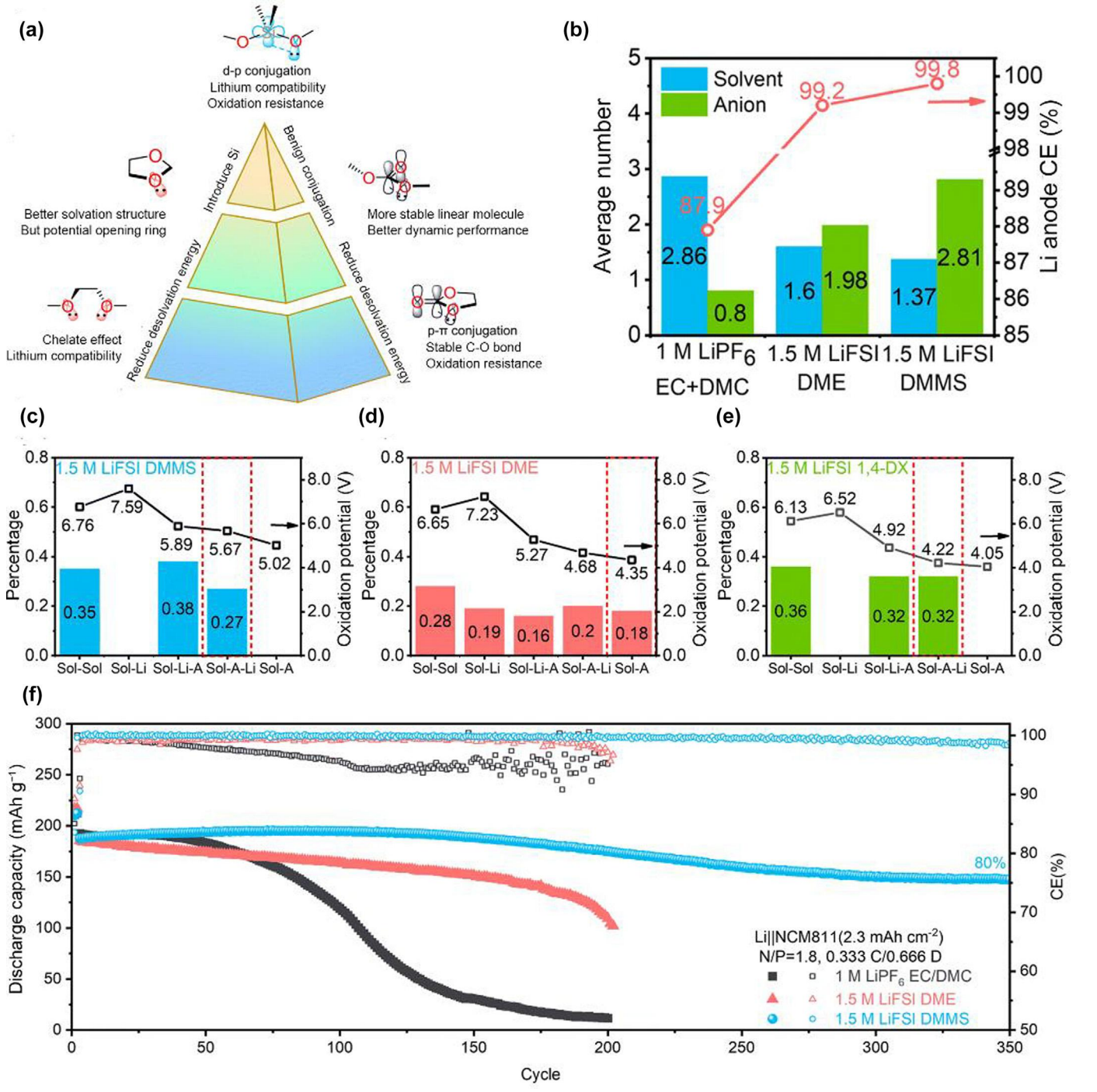

FIG. 7

The design principles, properties, and performances of siloxane electrolytes. (a) DMMS design principles (Reprinted with permission from Ref. [167]. Copyright 2022, The Royal Society of Chemistry.). (b) Average solvation structure and Li anode CE of the DMMS-based electrolyte compared with the conventional carbonate electrolyte and ether electrolyte (Reprinted with permission from Ref. [167]. Copyright 2022, The Royal Society of Chemistry.). The proportion and oxidation potentials of the five solvent clusters in (c) 1.5 M LiFSI DMMS, (d) 1.5 M LiFSI DME, and (e) 1.5 M LiFSI 1,4-DX. The minimum of the oxidation potentials of existent clusters in the electrolyte is framed by a red dashed line (Reprinted with permission from Ref. [167]. Copyright 2022, The Royal Society of Chemistry.). (f) Li anode full-cell performances (Reprinted with permission from Ref. [167]. Copyright 2022, The Royal Society of Chemistry.).

charge capacity after 350 cycles, with an average CE exceeding 99.9% (Fig. 7f).

Siloxane electrolytes exhibit high intrinsic electrochemical stability and an anion-rich solvation structure, contributing to their excellent performance in high-voltage LMBs. They also have characteristics of self-purifying, flame-retardant, and low density. However, the limited or absent solubility of certain siloxanes for lithium salts impedes their broader application. Ma et al. [182] proposed an electrolyte design strategy that overcomes the limitations associated with Li salt dissociation in silox-

ane solvents, namely 1,3-bis(trimethylsilyloxy)propane(BTP) and 1,2-bis(trimethylsilyloxy)ethane(BTE) (denoted as recessive solvents). BTP and BTE dissolve Li salts when blended with specific fluorinated benzene and halide alkane compounds (denoted as inducer solvents), due to the hydrogen bonding between recessive and inducer solvents. These intermolecular interactions induce the configurational change of recessive solvents and lower their ESP, thereby enabling a dynamic solvation-desolvation process that promotes Li^+ transfer kinetics. Additionally, the dynamic solvation-desolvation process reduces average Li^+ desolvation energy (–15.01 kcal mol^{-1}) and leads to the formation of anion-rich SEI due to Li^+-anion pairs. By adjusting intermolecular interactions, non-solvating solvents can be converted into weakly solvating solvents, providing novel ideas for designing emerging WSEs.

Summary and outlook

WSEs are crucial for advancing the practical application of high-voltage, fast-charging, and low-temperature LBs. WSEs feature an anion-rich solvation structure, which promotes the formation of inorganic-rich interphase compatible with Li metal and high-voltage cathodes. Together, theoretical simulations and spectroscopic analyses can elucidate the interactions between Li^+, solvents, and anions, as well as their derived solvation structure, thereby providing researchers with comprehensive formation mechanisms and characteristics of WSEs. Insights into the nanostructure mechanism are essential for designing solvent molecules. The extensive chemical space of solvent molecules offers opportunities for innovative design. Furthermore, tremendous efforts have been devoted to designing solvents for WSEs, such as linear ether, epoxide, fluorinated ether, fluorinated ester, and siloxane. However, a substantial gap remains between the composition, structure, and function, which hinders the rational design of WSE molecules. The following aspects still require further exploration.

(1) *Formation mechanism of the anion-rich solvation structure*. There are abundant anion-rich solvation structures in WSEs, with growing evidence linking it to electrolyte composition. However, a quantitative description of the relationship between composition and solvation structure is very lacking now. Currently, empirical parameters such as dielectric constant and DN can serve as solvation structure descriptors, though they remain qualitative. The solvation structure arises from the competition between solvent and anion for coordination with Li^+, yet the correlation between the relative strengths of Li^+–solvent and Li^+–anion interactions and the resulting solvation structure remains unclear. To establish a robust relationship between composition and structure, it is essential to both quantitatively describe the solvation structure and identify simple but effective descriptors.

(2) The *relationship between characteristics of WSEs and battery performance*. WSEs generally exhibit high-voltage, low-temperature, and fast-charging performance, which is related to the anion-rich solvation structure and weak solvating power. However, the effect of these characteristics on battery performance is complicated. Both SEIs and CEIs can be regulated by the solvation structure and significantly affect battery performance. However, the precise relationship between SEIs and CEIs and battery performance remains unclear. Simultaneously a precise regulation of solvation structure to obtain SEIs and CEIs with specific compositions and structures is still very challenging. Furthermore, the Li^+ desolvation process, which impacts both high-voltage and fast-charging performance, is closely related to the solvation structure and Li^+–solvent interactions, particularly at the interface. To establish the relationship between microstructure and performance, it is necessary to first determine how SEIs and CEIs composition and structure affect electrode performance. Next, the relationship between solvation structure and SEIs and CEIs composition and structure must be elucidated. Finally, developing a more accurate double-layer model is essential for describing solvation behavior at the interface.

(3) *Advanced characterization techniques*. The interactions between electrolyte components influence the solvation structure, ultimately impacting battery performance. The study of these interactions has primarily focused on strong interactions such as Li^+–solvent and Li^+–anion, while there are fewer studies on weak interactions such as anion–solvent and solvent–solvent. The study of weak interactions helps to achieve a complete description of the interactions between components. NMR, particularly two-dimensional NMR, can afford valuable insights into atomic-scale microscopic changes, especially useful for unveiling weak interactions. Additionally, research on solvation structures has mainly concentrated on the bulk phase, with limited studies on interfacial solvation structures. Observing the solvation structure at interfaces is crucial for understanding the solvation and desolvation processes. The development of new in situ characterization techniques is expected to address these challenges.

(4) *Comprehensive evaluation of the Ah-level battery performance of WSEs*. Safe and reliable performances are the prerequisites for the practical applications of full batteries. Currently, WSEs has been validated experimentally under fast-charging, high-voltage, and high energy density conditions. However, there has not been a systematic evaluation of the A- and B-level performances in the industry. Research on the safety evaluation, aging behavior, and self-discharge behavior of WSE battery systems remains lacking. Under fast-charging conditions, the battery temperature often rises, and the changes in internal resistance due to battery grouping have not yet been optimized for the design of battery packs and battery modules. A detailed evaluation is recommended to advance the development of practical WSE battery systems.

(5) *Li bond-inspired electrolyte chemistry discovery*. In the design of WSEs, current research mainly focuses on the Li ionic bond between Li^+ and solvent, as well as between Li^+ and anion. However, the possible presence of a Li bond between Li^+ and solvent, as well as between Li^+ and anion has received comparatively less attention. Recent studies [183] indicate that the Li bond plays a significant role in electrolytes, and its influence on the formation of solvation structure should not be overlooked. The Li bond is characterized as a dipole–dipole interaction that depends on electron localization effects, whereas the Li ionic bond is determined by an electrostatic interaction. A coordination number of 4 is crucial for distinguishing between the Li bond and the Li ionic bond. There are significant differences between the Li bond and Li ionic bond in terms of bond properties, coordination

number, bond energy, and bond length. Research on Li bond remains in its early stages. A comprehensive understanding of the Li bond will help to accurately control the solvation structure, thereby providing new possibilities for the practical applications of WSEs in rechargeable batteries.

(6) *AI-assisted rational design of WSEs*. Currently, WSEs are mainly designed through a costly and time-consuming trial-and-error approach. Artificial intelligence (AI) can quickly and accurately process large-scale data and make decisions based it. AI-assisted rational design of WSEs has the potential to accelerate their practical application in LBs. Graph theory algorithms can generate a huge molecule database, while high-throughput quantum-chemical calculations can effectively evaluate the properties of these molecules. Descriptors such as binding energy and redox stability can help narrow the molecular range based on the specific requirements of WSEs. However, some quantum-chemical calculations, such as dielectric constant and ionic conductivity, are both expensive and time-consuming. AI provides the possibility to establish structure–property relationships. Experiments are necessary to verify the properties of candidate solvents. To improve experimental efficiency and ensure repeatability of experimental results, AI-driven robotic experiments are very important. Through active learning, the robot can iteratively improve based on experimental data. AI-driven approaches enhance the efficiency of solvent molecular design, particularly in exploring unknown chemical spaces to discover molecules with desired properties. AI has significant advantages in processing massive data, and its integration with electrolyte theory and experimental research methods will strongly promote the development of the next generation of high energy, fast-charging, and wide temperature range batteries.

(7) *Generalization of the WSE concept*. The concept of WSEs was firstly proposed for lithium battery electrolytes, but it is supposed to be applied to other battery systems, such as sodium and multivalent-ion batteries. Currently, WSEs have made significant progress in sodium batteries, advancing the development of low-temperature and fast-charging sodium batteries [184–187]. WSEs can reduce the interaction between cations and solvent molecules, thereby facilitating the desolvation process of cations at the electrode interface. This characteristic is particularly important for multivalent-ion batteries, as the high charge density of multivalent-ion ions often results in a slow desolvation process at the electrode interface [188,189]. Although WSEs hold great potential for multivalent-ion batteries, they also face several challenges, such as the compatibility between electrolytes and anodes. By continually optimizing the performance of WSEs, it is expected that the commercial application of multivalent-metal batteries will be achieved in the future.

Vigorously developing renewable energy is the key to promoting sustainable development. Battery technology, as a representative of energy storage technology, has developed rapidly. Rational optimization of electrolytes is an important breakthrough in electrochemical energy storage. Solid-state electrolytes are currently highly valued worldwide and are considered an important technology for the future. Liquid electrolytes seem poised for replacement. However, since battery research in previous years was often based on processes and applications, the understanding of electrolyte structure and function was very superficial, resulting in electrolyte research often being like an art. WSEs can be seen as a new artistic genre, a system that has not been seriously considered or explored before. The molecules of the material world offer a vast array of options and bring about endless possibilities. We call for more researchers to enter this field, employing machine learning, experimental validation, rational design, and engineering intuition to accelerate innovation in electrolytes, making batteries safer, more powerful, more stable, and better serving humanity's pursuit of a better life.

CRediT authorship contribution statement

Yao-Peng Chen: Writing – review & editing, Writing – original draft, Visualization, Validation, Software, Resources, Investigation, Formal analysis, Data curation, Conceptualization. **Xiang Chen:** Writing – review & editing, Writing – original draft, Visualization, Validation, Supervision, Project administration, Investigation, Funding acquisition, Formal analysis, Data curation, Conceptualization. **Nan Yao:** Writing – review & editing, Writing – original draft, Methodology, Investigation, Data curation, Conceptualization. **Zhao Zheng:** Writing – review & editing, Writing – original draft, Project administration, Methodology, Investigation, Formal analysis, Data curation, Conceptualization. **Legeng Yu:** Writing – review & editing, Writing – original draft, Resources, Project administration, Methodology, Formal analysis, Data curation, Conceptualization. **Yu-Chen Gao:** Writing – review & editing, Writing – original draft, Visualization, Validation, Software, Investigation, Funding acquisition, Formal analysis, Data curation. **Han-Bing Zhu:** Writing – review & editing, Writing – original draft, Validation, Project administration, Methodology, Investigation, Formal analysis, Data curation. **Chao-Long Wang:** Writing – review & editing, Writing – original draft, Visualization, Methodology, Formal analysis. **Jin-Hao Yao:** Writing – review & editing, Writing – original draft, Visualization, Investigation, Formal analysis, Data curation. **Qiang Zhang:** Writing – review & editing, Writing – original draft, Visualization, Validation, Resources, Investigation, Funding acquisition, Formal analysis, Data curation, Conceptualization.

Data availability

Data will be made available on request.

Declaration of competing interest

The authors declare that they have no known competing financial interests or personal relationships that could have appeared to influence the work reported in this paper.

Acknowledgments

This work was supported by Beijing Municipal Natural Science Foundation (L233004, L247015), Huaneng Group Science and Technology Research project (HNKJ23-H71), National Natural Science Foundation of China (T2322015, 22109007, 22393900, 22109011, 52394170, 52394171, 22109086, 22209010, and 22108151), Tsinghua University Initiative Scientific Research Program.

References

[1] M. Armand et al., Nature 451 (2008) 652–657.
[2] E.C. Evarts, Nature 526 (2015) S93–S95.
[3] J.W. Choi et al., Nat. Rev. Mater. 1 (2016) 16013.
[4] Y. Sun et al., Nat. Energy 1 (2016) 16071.
[5] J. Xiao, Science 366 (2019) 426–427.
[6] X.-B. Cheng et al., Chem. Rev. 117 (2017) 10403–10473.
[7] J. Liu et al., Nat. Energy 4 (2019) 180–186.
[8] J.-G. Zhang et al., Chem. Rev. 120 (2020) 13312–13348.
[9] M. Winter et al., Chem. Rev. 118 (2018) 11433–11456.
[10] B. Liu et al., Joule 2 (2018) 833–845.
[11] J.M. Tarascon et al., Nature 414 (2001) 359–367.
[12] D. Lin et al., Nat. Nanotechnol. 12 (2017) 194–206.
[13] C.-X. Zhao et al., Nat. Chem. Eng. 1 (2024) 251–260.
[14] Y.-W. Song et al., Nat. Chem. Eng. 1 (2024) 588–596.
[15] Z. Cui et al., Energy Storage Mater. 57 (2023) 14–43.
[16] A.V. Ivanishchev et al., J. Electroanal. Chem. 860 (2020) 113894.
[17] A. Manthiram et al., Adv. Energy Mater. 6 (2016) 1501010.
[18] S.-T. Myung et al., ACS Energy Lett. 2 (2017) 196–223.
[19] H.-J. Noh et al., J. Power Sources 233 (2013) 121–130.
[20] J. Xiang et al., Adv. Mater. 34 (2022) 2200912.
[21] L. Zhang et al., Solid State Ion 387 (2022) 116062.
[22] J. Li et al., J. Electrochem. Soc. 162 (2015) A1401.
[23] F.A. Soto et al., Chem. Mater. 27 (2015) 7990–8000.
[24] S.K. Heiskanen et al., Joule 3 (2019) 2322–2333.
[25] A. Wang et al., npj Comput. Mater. 4 (2018) 15.
[26] K. Xu, Chem. Rev. 104 (2004) 4303–4418.
[27] K. Xu, Chem. Rev. 114 (2014) 11503–11618.
[28] H. Wu et al., Adv. Energy Mater. 11 (2021) 2003092.
[29] B. Jagger et al., Joule 7 (2023) 2228–2244.
[30] K. Xu, J. Power Sources 559 (2023) 232652.
[31] H. Wan et al., Nat. Rev. Chem. 8 (2024) 30–44.
[32] J. Song et al., Adv. Energy Mater. 8 (2018) 1703082.
[33] C. Yan et al., Adv. Funct. Mater. 30 (2020) 1909887.
[34] P. Xiao et al., Chem. Soc. Rev. 52 (2023) 5255–5316.
[35] M. Gauthier et al., J. Phys. Chem. Lett. 6 (2015) 4653–4672.
[36] K. Xu et al., J. Non-Cryst. Solids 14 (2022) 100088.
[37] O. Borodin et al., Joule 4 (2020) 69–100.
[38] G.A. Giffin, Nat. Commun. 13 (2022) 5250.
[39] Y. Yamada et al., Nat. Energy 4 (2019) 269–280.
[40] Q.-K. Zhang et al., Nat. Energy 8 (2023) 725–735.
[41] Y.S. Meng et al., Science 378 (2022) eabq3750.
[42] J. Zheng et al., ACS Energy Lett. 3 (2018) 315–321.
[43] X. Cao et al., J. Electrochem. Soc. 168 (2021) 010522.
[44] Y. Yamada et al., J. Electrochem. Soc. 162 (2015) A2406.
[45] H. Wang et al., Joule 6 (2022) 588–616.
[46] J. Zheng et al., Adv. Sci. 4 (2017) 1700032.
[47] X. Ren et al., Joule 3 (2019) 1662–1676.
[48] C. Tian et al., Mater. Futures 2 (2022) 012101.
[49] A.-M. Li et al., Nat. Chem. 16 (2024) 922–929.
[50] K. Xu et al., Langmuir 26 (2010) 11538–11543.
[51] T. Ma et al., Angew. Chem. Int. Ed. 134 (2022) e202207927.
[52] Y.X. Yao et al., Angew. Chem. Int. Ed. 60 (2021) 4090–4097.
[53] R. Hou et al., Adv. Energy Mater. 13 (2023) 2300053.
[54] Z. Li et al., Angew. Chem. Int. Ed. 62 (2023) e202303888.
[55] Y. Mo et al., Next Energy 3 (2024) 100115.
[56] Y. Liu et al., Nat. Energy 4 (2019) 540–550.
[57] X. Fan et al., Chem. Soc. Rev. 50 (2021) 10486–10566.
[58] G. Leverick et al., Adv. Energy Mater. 13 (2023) 2204094.
[59] Z. Piao et al., Adv. Mater. 35 (2023) 2206009.
[60] Z. Wang et al., Energy Mater. Devices 1 (2023) 9370003.
[61] M. Ma et al., Interdisc. Mater. 2 (2023) 833–854.
[62] M. Qin et al., Adv. Funct. Mater. 34 (2024) 2406357.
[63] Z. Jiang et al., Energy Environ. Mater. 6 (2023) e12440.
[64] J.F. Ding et al., Angew. Chem. Int. Ed. 60 (2021) 11442–11447.
[65] L. Sheng et al., Nano Lett. 24 (2023) 533–540.
[66] Q. Zhao et al., Angew. Chem. Int. Ed. 61 (2022) e202116214.
[67] P. Lai et al., Energy Storage Mater. 67 (2024) 103314.
[68] Y. Wu et al., Adv. Energy Mater. 13 (2023) 2300259.
[69] M. Baek et al., Adv. Mater. 32 (2020) 2005022.
[70] H. Chu et al., Nat. Commun. 10 (2019) 188.
[71] L. Johnson et al., Nat. Chem. 6 (2014) 1091–1099.
[72] X. Gao et al., Nat. Mater. 15 (2016) 882–888.
[73] J. Chen et al., ACS Energy Lett. 8 (2023) 1723–1734.
[74] H. Hu et al., J. Energy Chem. 98 (2024) 374–382.
[75] W. Earle Waghorne et al., J. Solut. Chem. 47 (2018) 1609–1625.
[76] C.-C. Su et al., Energy Environ. Sci. 12 (2019) 1249–1254.
[77] J. Xu et al., Nature 614 (2023) 694–700.
[78] X. Chen et al., Batteries Supercaps 2 (2019) 128–131.
[79] X. Li et al., Carb. Neutrality 2 (2023) 34.
[80] K. Chen et al., Angew. Chem. Int. Ed. 62 (2023) e202312373.
[81] N. Yao et al., Angew. Chem. Int. Ed. 62 (2023) e202305331.
[82] X. Chen et al., Acc. Chem. Res. 53 (2020) 1992–2002.
[83] X. Chen et al., Angew. Chem. Int. Ed. 57 (2018) 16643–16647.
[84] X. Chen et al., Angew. Chem. Int. Ed. 57 (2018) 734–737.
[85] M. Shakourian-Fard et al., ChemPhysChem 17 (2016) 2916–2930.
[86] J. Zhang et al., Phys. Chem. Chem. Phys. 23 (2021) 20323–20328.
[87] Y.-C. Gao et al., J. Am. Chem. Soc. 145 (2023) 23764–23770.
[88] J. Self et al., ACS Energy Lett. 4 (2019) 2843–2849.
[89] O. Borodin et al., ACS Nano 11 (2017) 10462–10471.
[90] O. Borodin et al., J. Phys. Chem. C 122 (2018) 20108–20121.
[91] N. Yao et al., Angew. Chem. Int. Ed. 60 (2021) 21473–21478.
[92] M.T. Ong et al., J. Phys. Chem. B 119 (2015) 1535–1545.
[93] T.A. Pham et al., J. Phys. Chem. C 121 (2017) (1920) 21913–121912.
[94] S.H. Lapidus et al., Phys. Chem. Chem. Phys. 16 (2014) (1945) 21941–21942.
[95] B. Ravikumar et al., J. Phys. Chem. C 122 (2018) 8173–8181.
[96] W. Wahyudi et al., Adv. Funct. Mater. 31 (2021) 2101593.
[97] I. Ruggeri et al., ChemElectroChem 6 (2019) 4002–4009.
[98] X. Bogle et al., J. Phys. Chem. Lett. 4 (2013) 1664–1668.
[99] W. Wahyudi et al., Adv. Sci. 9 (2022) 2202405.
[100] Y. Yamada et al., J. Am. Chem. Soc. 136 (2014) 5039–5046.
[101] J. Zhang et al., ACS Energy Lett. 5 (2020) 3124–3131.
[102] D.M. Seo et al., J. Phys. Chem. C 119 (2015) 14038–14046.
[103] C.M. Efaw et al., Nat. Mater. 22 (2023) 1531–1539.
[104] Z. Li et al., Nat. Commun. 14 (2023) 868.
[105] Z. Wang et al., ACS Nano 17 (2023) 18103–18113.
[106] X. Kong et al., J. Power Sources 551 (2022) 232211.
[107] J. Holoubek et al., Nat. Energy 6 (2021) 303–313.
[108] H. Zhang et al., Angew. Chem. Int. Ed. 62 (2023) e202300771.
[109] T. Ma et al., Angew. Chem. Int. Ed. 62 (2023) e202310761.
[110] E. Park et al., ACS Energy Lett. 8 (2023) 179–188.
[111] T. Ma et al., Angew. Chem. Int. Ed. 61 (2022) e202207927.
[112] S. Chen et al., Angew. Chem. Int. Ed. 62 (2023) e202219310.
[113] J.-L. Liang et al., Sci. China Chem. 66 (2023) 3620–3627.
[114] S. Chen et al., ACS Appl. Mater. Interfaces 15 (2023) 13155–13164.
[115] J. Kim et al., J. Phys. Chem. C 125 (2021) 4614–4622.
[116] Y. Zhang et al., Adv. Funct. Mater. 34 (2024) 2315527.
[117] X. Liu et al., Angew. Chem. Int. Ed. 63 (2024) e202406596.
[118] A. Dutta et al., Adv. Sci. 11 (2024) 2404245.
[119] D. Xia et al., Adv. Energy Mater. 14 (2024) 2400773.
[120] Z. Yu et al., Adv. Funct. Mater. 34 (2024) 2315446.
[121] M. Gu et al., Angew. Chem. Int. Ed. 63 (2024) e202402946.
[122] Z. Wang et al., Angew. Chem. Int. Ed. 62 (2023) e202303950.
[123] S. Wang et al., Angew. Chem. Int. Ed. 62 (2023) e202313447.
[124] Y. Chen et al., J. Am. Chem. Soc. 143 (2021) 18703–18713.
[125] T.D. Pham et al., Small 17 (2021) 2100133.
[126] T.D. Pham et al., Small 18 (2022) 2107492.
[127] Z. Huang et al., Angew. Chem. Int. Ed. 131 (2019) 2367–2371.
[128] Y. Liao et al., Adv. Energy Mater. 13 (2023) 2301477.
[129] Y.-X. Yao et al., Angew. Chem. Int. Ed. 60 (2021) 4090–4097.
[130] J. Zhang et al., ACS Energy Lett. 8 (2023) 1752–1761.
[131] Y. Yang et al., Angew. Chem. Int. Ed. 136 (2024) e202409193.
[132] N. Piao et al., J. Am. Chem. Soc. 146 (2024) 18281–18291.
[133] Y. Liao et al., ACS Nano 18 (2024) 20762–20771.
[134] Y. Wang et al., Nat. Rev. Mater. 9 (2024) 119–133.
[135] Y. Wang et al., Chem. Soc. Rev. 52 (2023) 2713–2763.
[136] X. Cao et al., Nat. Energy 4 (2019) 796–805.
[137] J. Chen et al., Angew. Chem. Int. Ed. 63 (2024) e202317923.
[138] S. Chen et al., Joule 2 (2018) 1548–1558.
[139] Y. Zhao et al., ACS Energy Lett. 8 (2023) 3180–3187.
[140] Y. Zhao et al., Nat. Commun. 14 (2023) 299.
[141] Y. Lin et al., J. Mater. Chem. A 12 (2024) 2986–2993.
[142] L.-Q. Wu et al., J. Am. Chem. Soc. 146 (2024) 5964–5976.
[143] G. Zhang et al., Nat. Commun. 14 (2023) 1081.
[144] Z. Yu et al., Nat. Energy 5 (2020) 526–533.

[145] Z. Yu et al., Nat. Energy 7 (2022) 94–106.
[146] C.V. Amanchukwu et al., J. Am. Chem. Soc. 142 (2020) 7393–7403.
[147] Z. Cui et al., Nat. Commun. 15 (2024) 2033.
[148] Z. Zhao et al., Angew. Chem. Int. Ed. (2024) e202412239.
[149] H. Wang et al., Adv. Mater. 33 (2021) 2008619.
[150] Y. Mo et al., Adv. Energy Mater. 13 (2023) 2301285.
[151] Y. Zhang et al., Langmuir 36 (2020) 11450–11466.
[152] W. Zhang et al., Energy Storage Mater. 57 (2023) 249–259.
[153] Y. Yang et al., Angew. Chem. Int. Ed. 61 (2022) e202208345.
[154] X. Yang et al., J. Phys. Chem. B 127 (2023) 3026–3040.
[155] M. Mao et al., Nat. Commun. 14 (2023) 1082.
[156] J. Holoubek et al., ACS Energy Lett. 5 (2020) 1438–1447.
[157] L. Deng et al., Adv. Energy Mater. 14 (2024) 2303652.
[158] Z. Cao et al., ACS Energy Lett. 7 (2022) 3581–3592.
[159] W. Cai et al., Adv. Energy Mater. 13 (2023) 2301396.
[160] W. Yang et al., Angew. Chem. Int. Ed. (2024) e202410893.
[161] Y. Wang et al., Nat. Commun. 15 (2024) 5408.
[162] M. Qin et al., Adv. Funct. Mater. (2024) 2406357.
[163] D.-J. Yoo et al., Adv. Energy Mater. 13 (2023) 2204182.
[164] Z. Yu et al., J. Electrochem. Soc. 169 (2022) 040555.
[165] J. Wu et al., ACS Appl. Mater. Interfaces 14 (2022) 27873–27881.
[166] H. Ma et al., Chem. Eng. J. 479 (2024) 147557.
[167] Y. Huang et al., Energy Environ. Sci. 15 (2022) 4349–4361.
[168] H. Zhang et al., Angew. Chem. Int. Ed. 62 (2023) e202218970.
[169] M. Xia et al., J. Power Sources 548 (2022) 232106.
[170] C. Sun et al., ACS Energy Lett. 8 (2023) 4119–4128.
[171] Z. Piao et al., J. Am. Chem. Soc. 145 (2023) 24260–24271.
[172] H. Lu et al., Energy Storage Mater. 63 (2023) 102994.
[173] D. Lu et al., Energy Environ. Sci. 15 (2022) 3331–3342.
[174] T. Liu et al., Adv. Mater. 33 (2021) 2102034.
[175] Y. Li et al., Adv. Energy Mater. 13 (2023) 2300918.
[176] M. Li et al., J. Mater. Chem. A 11 (2023) 11721–11729.
[177] L. Xing et al., J. Phys. Chem. A 115 (2011) 13896–13905.
[178] Y. Wang et al., J. Am. Chem. Soc. 123 (2001) 11708–11718.
[179] T. Li et al., J. Power Sources 244 (2013) 668–674.
[180] S.A. Delp et al., Electrochim. Acta 209 (2016) 498–510.
[181] O. Borodin et al., J. Phys. Chem. C 117 (2013) 8661–8682.
[182] B. Ma et al., Nat. Chem. 16 (2024) 1–9.
[183] N. Yao et al., Chem 11 (2025) 102254.
[184] M. Wu et al., J. Am. Chem. Soc. (2024).
[185] S. Wang et al., J. Am. Chem. Soc. 146 (2024) 3854–3860.
[186] C. Wang et al., Nat. Commun. 15 (2024) 6292.
[187] C. Hu et al., Angew. Chem. Int. Ed. 63 (2024) e202407075.
[188] Y. Tian et al., Chem. Rev. 121 (2021) 1623–1669.
[189] Y. Liang et al., Nat. Energy 5 (2020) 646–656.